Check for updates

Comparison on the immersion corrosion and electrochemical corrosion resistance of WC–Al₂O₃ composites and WC–Co cemented carbide in NaCl solution

Bin Han,[a] Weiwei Dong,[a] Bowen Fan[a] and Shigen Zhu (ID) *[ab]

WC–15 wt% Al₂O₃ composites were prepared *via* hot pressing sintering technology. The corrosion behaviors of WC–Al₂O₃ composites and traditional WC–Co cemented carbide in NaCl solution were studied by immersion corrosion and electrochemical technique. The impedance value of the WC–Al₂O₃ composite increased more rapidly than WC–Co cemented carbide during the 24 hours, which indicated that WC–Al₂O₃ composites had a more compact passivation film than WC–Co cemented carbide. The results confirmed that the corrosion resistance of WC–Al₂O₃ composites was higher than that of WC–Co cemented carbide in NaCl solution. The corrosion mechanisms of WC–Al₂O₃ composites and WC–Co cemented carbide in NaCl solution were also revealed by SEM, EDS, XPS and Raman. The corrosion products of WC–Al₂O₃ composites mainly contain WO₃, while for WC–Co cemented carbide they are Co(OH)₂, Co₃O₄ and WO₃. The different corrosion mechanism of the two materials is attributed to the Al₂O₃ phase instead of the Co binder, which avoids the galvanic corrosion between the WC phase and the Co binder.

1. Introduction

Conventional WC-based hardmetals consist of a WC phase and a metal binder (Fe, Co, Ni, *etc.*), which could lead to high hardness and fracture toughness of hardmetals.[1–6] Among the conventional WC-based hardmetals, because the metal binder is chemically active and susceptible to corrosion, the development of binderless WC-based hardmetals has become an inevitable demand. Binderless WC-based hardmetals refer to the hard material without or with a small amount of metal binder (<0.5%, mass fraction), which is a new hard material in recent years. Binderless WC-based hardmetals can be used as special sealing materials (such as sealing materials for cooling water pumps in nuclear power stations, sealing materials for petroleum and chemical equipment in acidic and alkaline corrosion environments, *etc.*), high-pressure jet nozzles, fluid mixers, drilling part and valves.[7–9] Our group has previously developed the WC–Al₂O₃ composite as a new type of binderless WC-based hardmetals and carried out a series of studies. The research content includes: the ratio of WC and Al₂O₃ composition,[10] crystal type and morphology of Al₂O₃,[11] sintering process parameters and two-stage hot pressing sintering process,[12,13] rare earth materials,[14,15] grain growth inhibitor.[16,17] Through

these studies, WC–Al₂O₃ composite with excellent comprehensive mechanical properties have been prepared, which has attracted worldwide attention.

The corrosion resistance of materials used in corrosive environment is a very important technical index, which is usually studied by electrochemical method. Electrochemical corrosion resistance of WC-based hardmetals depends on several factors, which includes the binder composition,[18,19] WC grain size,[20–22] binder content[23] and additives.[24,25] Human *et al.*[23] confirmed that WC–Co cemented carbide possessed the higher anti-corrosion ability with the decrease of Co content. However, in his other research, it was concluded that the binder phase content had no influence on the corrosion resistance of hardmetals.[26] Studies on the corrosion behaviors of binderless hardmetals have been rarely reported in domestic and foreign literatures, mainly involving WC–TiC–TaC composite, WC–MgO composite.[27,28] Ma Y. *et al.*[27] studied the corrosion resistance of WC–TiC–TaC composite in NaCl solution, and believed that TiC and TaC could form solid solution with WC, which increased the resistivity and resistance of binderless WC-based hard composite and enhanced the corrosion resistance of the composites. Ouyang Chenxin *et al.*[28] studied the corrosion resistance of WC–MgO composite by immersion corrosion and electrochemical methods in alkaline (pH = 13) and acidic (pH = 1) environments, and believed that the corrosion resistance of WC–MgO composites in acidic environment was better than in alkaline environment. Passivation occurred in acidic environment, while no passivation occurred in alkaline environment.

[a]*College of Mechanical Engineering, Donghua University, Shanghai, 201620, PR China. E-mail: sgzhu@dhu.edu.cn*

[b]*Engineering Research Center of Advanced Textile Machinery of the Ministry of Education, Shanghai, 201620, PR China*

In this work, WC–Al$_2$O$_3$ composites was obtained *via* hot pressing sintering technology. However, the corrosion resistance of WC–Al$_2$O$_3$ composites in NaCl solution has not been reported. Therefore, the immersion corrosion and electrochemical corrosion resistance of WC–Al$_2$O$_3$ composite in NaCl solution compared to WC–Co hardmetal were researched.

2.   Experimental procedure

2.1   Sample preparation

WC–Al$_2$O$_3$ composite used in this work was fabricated by our group. Table 1 presented the compositions of WC-based composites. Raw materials of WC, Al$_2$O$_3$ (75 μm, 150 μm, respectively) and WC–6Co hardmetal were used in this work. The preparation process of WC–Al$_2$O$_3$ composite have been reported in our previous research by Zhu *et al.*[10] All the samples used for electrochemical corrosion tests were cut into squares from the hot-pressing sintered samples. The exposed area of the electrochemical corrosion samples is 1 cm^2.

2.2   Immersion corrosion test

According to ASTM standard G31-2004, the specimens were immersed in NaCl solution at 25 °C for obtaining the corrosion rate and macro corrosion morphologies of WC–Co hardmetal and WC–Al$_2$O$_3$ composite, respectively. The mass loss after immersion corrosion each stage (7 days, 14 days, 21 days and 28 days, respectively) was weighed for calculating the corrosion rates. Then the optical images of corroded surface after 7 days were observed by digital camera.

2.3   Electrochemical measurements

Electrochemical corrosion tests were conducted in NaCl solution at 25 °C and open to air. The electrolyte solution was prepared from sodium chloride crystals and distilled water. Tafel curves, EIS and OCP were measured by electrochemical workstation (CS310H, Wuhan Corrtest Instruments Corp., Ltd). The schematic diagram of the electrochemical three-electrode system is shown in Fig. 1. Saturated calomel electrode was used as the reference electrode. WC matrix composite was used as working electrode. Platinum sheet was used as counter electrode. The area of the electrodes is 1 cm^2. The open circuit potential curves were monitored for about 12 h in NaCl solution. Subsequently, the EIS test was conducted on the position of OCP value. The test frequency ranged from 100 kHZ to 1 mHZ. The potentiodynamic polarization was measured in the potential range from −1000 mV *vs.* SCE to +1500 mV *vs.* SCE. Refer to the experimental parameters of Konadu *et al.*[38] The
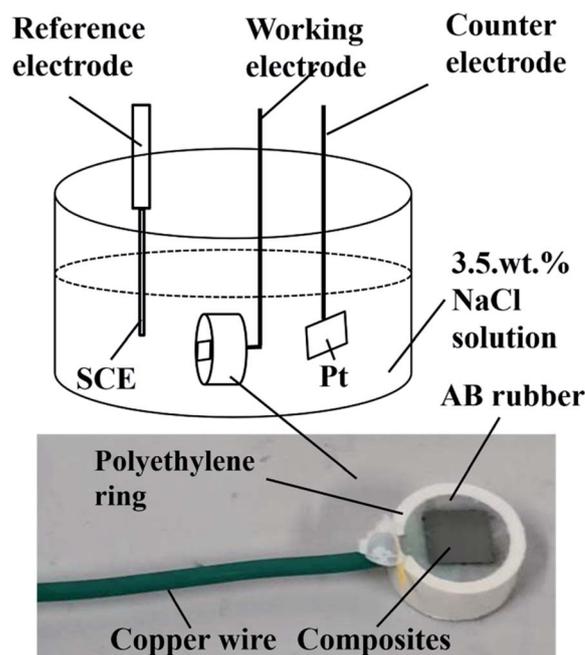

Fig. 1   The schematic diagram of the electrochemical testing system.

scanning rate for all the samples was 2 mV s^{-1}. This scanning rate is typical of those used in literature even though higher scan rates of 5 mV s^{-1} (ref. 29) has been reported. The scan rate used is not important since the scan rate does not affect the qualitative results.[30]

2.4   Microstructural and composition characterization

Prior to microstructural characterization, the specimens were ground with diamond discs from 600 grit to 4000 grit and polished with 1 μm diamond pastes. Then the sample surface was degreased in ethanol by using ultrasonic cleaner. The microstructure and chemical composition of the specimens were observed by SEM (Quanta 250, FEI Co. Ltd., USA) and EDS (AZtec X-Max 20, Oxford Co. Ltd., UK). The phase composition of the specimens was characterized by XRD (D/max-2550PC, Rigaku Co. Ltd., Japan) and Raman spectroscopy (inVia-Reflex, Renishaw Co. Ltd., UK). The composition of the corrosion products of the composites after corrosion test was determined by XPS (Escalab 250Xi, China). The binding energy of C 1s standard carbon was used as the reference peak. XPS spectrum is fitted by XPS peak software.

3.   Results and discussion

3.1   Microstructure characterization before corrosion tests

The XRD pattern of WC–Co hardmetal and WC–Al$_2$O$_3$ composite are shown in Fig. 2. The local magnified XRD pattern of Fig. 2(a) was faintly observed in Fig. 2(b). In both materials of WC–Co and WC–Al$_2$O$_3$, WC is the main peak. The weak Al$_2$O$_3$ and Co peaks also can be observed, respectively. WC–Al$_2$O$_3$ composite has no phase transition after hot pressing sintering.

Table 1   The compositions of the WC-based composites

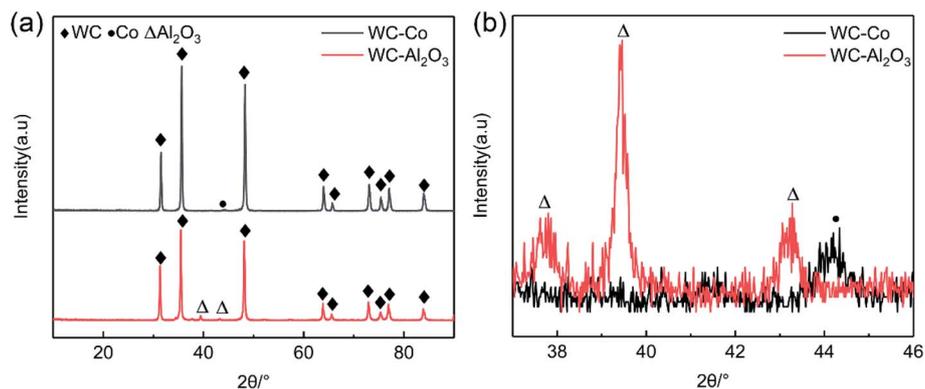|	Composition (wt%)		
	WC	Co	Al$_2$O$_3$
WC–6Co	94	6	—
WC–15Al$_2$O$_3$	85	—	15

Fig. 2 XRD pattern of the polished composites: (a) polished samples; (b) local XRD patterns.

It can be seen that WC peak is higher intense than Al_2O_3 and Co peak due to the low amount of Al_2O_3 and Co.

BSE-SEM images of the polished samples are presented in Fig. 3. The uniform microstructure was observed in the sample. As shown in Fig. 3(a), WC–Al_2O_3 composite is almost completely compact, which indicates that densification has occurred in the sample during the sintering process. WA15 composite had the double phase microstructure. Dark regions are dispersed Al_2O_3 particles and the surrounding bright regions are WC particles. The microstructure, mechanical performance and frictional wear properties of WC–Al_2O_3 composite have been reported in our pervious study by Qu et al.[11] As presented in Fig. 3(b), Co binder is visible in the WC–Co hardmetal, which uniformly surrounds the WC particles.

3.2 Corrosion behavior after immersion corrosion test

Fig. 4(a) and (b) illustrates the optical morphologies of WC–Co hardmetal and WC–Al_2O_3 composite after immersion tests for 7 days in NaCl solution, respectively. As presented in Fig. 4(a), obvious corrosion products appeared on the surface of WC–Co hardmetal. However, as presented in Fig. 4(b), no corrosion layer was visible on the corroded surface of WC–Al_2O_3 composite. Fig. 4(c) shows the mass loss curve of the samples after immersion corrosion test for 7, 14, 21 and 28 days,

respectively. It could be found that the dissolution rate increased obviously with immersion time in the sample of WC–Co hardmetal. However, there were no significant differences in WC–Al_2O_3 composite at any time point. Hence, it may be speculated that the corrosion resistance of WC–Al_2O_3 composite in NaCl solution is higher than WC–Co hardmetal. Human et al.[23] have reported the corrosion mechanism of WC–Co hardmetal in NaCl solution, while for WC–Al_2O_3 composite was not yet clear.

3.3 Electrochemical response

3.3.1 OCP monitoring. Fig. 5 shows the OCP curves of all specimens measured in NaCl solution for 12 h. The open circuit potential becomes stable with immersion time, which implies that the corroded surface of WC-based composites is stable gradually and not easily affected to pitting in electrolyte solution.[31] As shown in Fig. 5, WC–Al_2O_3 composites possesses more positive E_{OCP} value than WC–Co hardmetal. Katiyar et al.[31] reported that the higher positive E_{OCP} value implies the lower tendency to corrode from corrosion thermodynamics. The E_{OCP} value of WC–Al_2O_3 composite increases slightly with immersion time. This indicates that the passive film becomes compact at the final stage of immersion, which could hinder further corrosion of WC–Al_2O_3 composite.[32] For WC-Co cemented
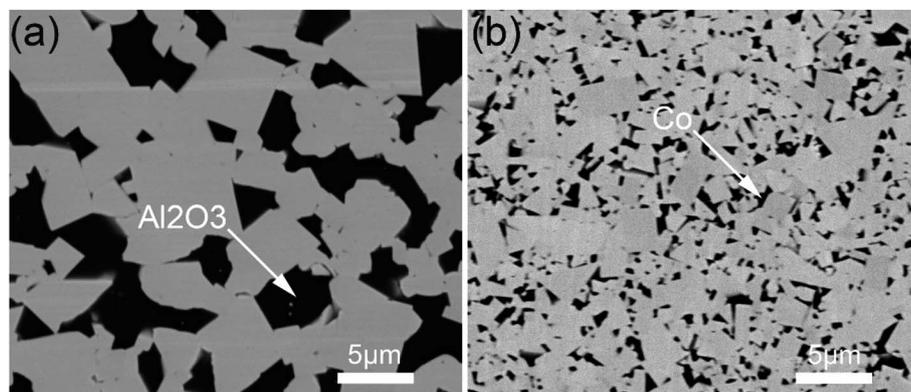

Fig. 3 BSE-SEM images of the sintered samples: (a) WC–Al_2O_3 composite; (b) WC–Co hardmetal.
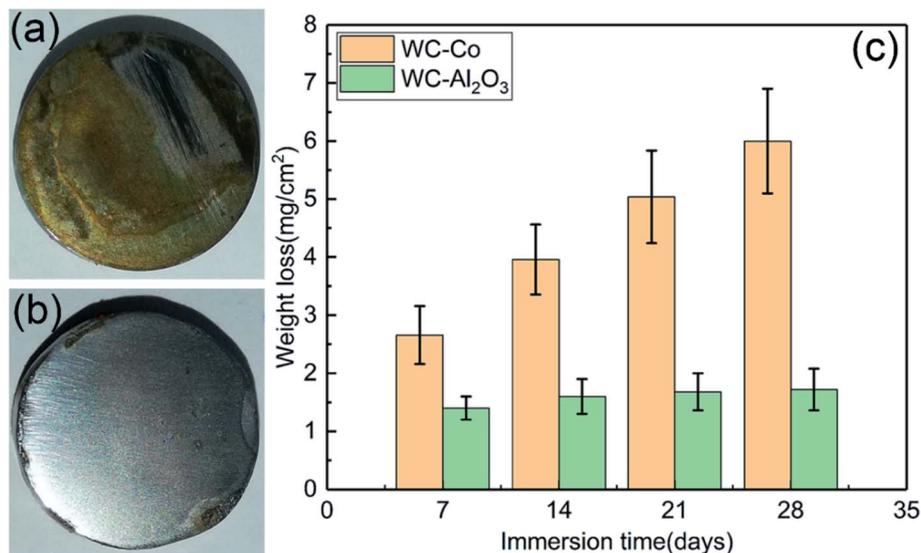
Fig. 4 Optical images (a and b), and mass loss (c) of WC−Co and WC−Al$_2$O$_3$ specimens after immersion corrosion test in NaCl solution.
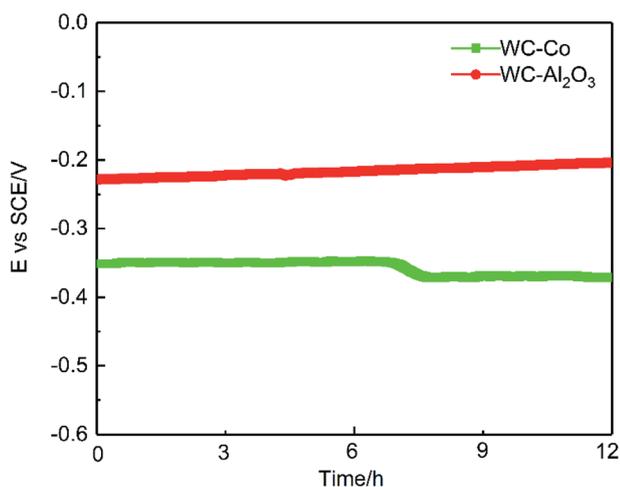

Fig. 5 OCP measurements of the polished samples.

anodic behavior. The corrosion current density (i_{corr}) increases exponentially with the corrosion potential (E_{corr}). Subsequently, it tends to the steady state.[32] The cathodic polarization branches display the oxygen reaction in NaCl solution. This phenomenon is controlled by activation in WC-based composites. All the composites exhibit the passivation behavior, which was marked by the decrease or almost constant in the corrosion current density at higher potentials. In the anodic polarization curve, WC–Al$_2$O$_3$ composite shows the passivation behavior and the passivation current density (i_{pass}) is less than 10 μA cm^{-2}.[23] However, WC–Co cemented carbide exhibits the pseudo-passivation behavior, because the passivation current density (i_{pass}) is much higher than 10 μA cm^{-2}. The pseudo-passivation behaviors occurred when the pseudo-passivation current density of the composite at higher potential was several orders of magnitude higher than the passivation current density. The pseudo-passivation observed here for WC–Co hardmetal is

carbide, with the increase of immersion time, the E_{OCP} value tended to stabilize firstly and then decrease. In the initial 7 hours, the E_{OCP} value remained basically unchanged, which indicated that the corrosion trend remained unchanged in this stage, but after immersion for 7 hours, the E_{OCP} value showed a downward trend, which indicated that there was a higher corrosion trend in this stage. The decrease of E_{OCP} value indicated that WC–Co cemented carbide had active dissolution. Because the corrosion potential of WC phase is more positive than the Co binder, the Co ions are preferred to enter the electrolyte.[39,40] Hence, it could be speculated that the corrosion stability of WC–Al$_2$O$_3$ composites was higher than WC–Co hard metal by replacing the Co binder with Al$_2$O$_3$ particle.

3.3.2 Tafel curves. Fig. 6 presents the Tafel curves of WC–Al$_2$O$_3$ composites and WC–Co hardmetal in NaCl solution. The polarization curves of WC-based composites indicate the typical
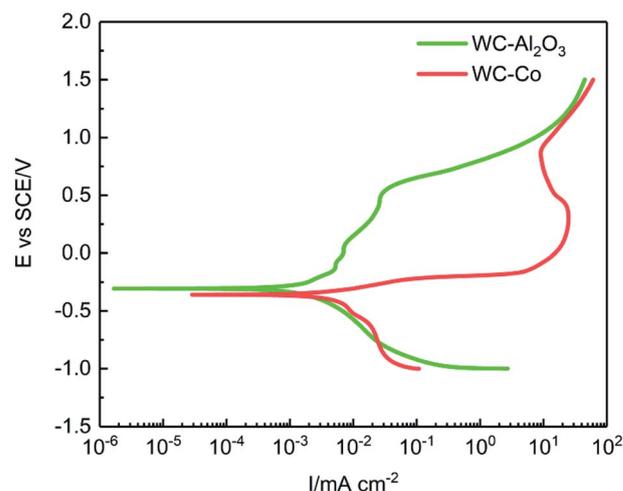

Fig. 6 Tafel curves of the polished specimens in NaCl solution.

Table 2 The corrosion parameters of the composites in NaCl solution

Samples	E_{OCP} (vs. SCE, mV)	E_{corr} (vs. SCE, mV)	i_{corr} (µA cm^{-2})	i_{pass} (µA cm^{-2})
WC–6Co	−376.2	−359.6	18.25	2020.4
WC–15Al$_2$O$_3$	−238.8	−312.1	32.56	8.55

consistent with other reported study.[33] On one hand, Co binder has a low corrosion potential compared with WC phase,[33] so it can be said that Co binder has the priority of dissolution, and WC phase is protected by the cathode. On the other hand, WC phase could be oxidized at anodic potential. Therefore, the oxidation of WC phase and active dissolution of Co binder could take place in NaCl solution.

Table 2 presents the corrosion parameters from the OCP and Tafel curves. There is a difference between the value of the open circuit potential and the corrosion potential. The open circuit potential is the electrode potential when no voltage is applied, and the corrosion potential is the potential obtained during the potential scanning process. During the scanning process, the electrode surface is corroded, so there is a difference between the open circuit potential and the corrosion potential. The significant corrosion parameters were obtained according to ASTM standard G5-94. The i_{corr} and E_{corr} were determined by Tafel extrapolation. The E_{corr} value reflected the thermodynamic characteristic of the composites.[34] Martin et al.[35] reported that the higher corrosion potential implies better chemical stability and lower corrosion tendency, and the lower i_{corr} reflects lower corrosion rate. It could be observed that the E_{corr} of WC–Al$_2$O$_3$ composite was higher than that of WC–Co hardmetal, implying that WC–Co hardmetal has lower corrosion tendency. Because the i_{corr} values can imply the dynamics characteristic of corrosion process, the i_{corr} value reflects the corrosion rate more accurately than E_{corr} value. WC–Al$_2$O$_3$ composite shows the lower i_{corr} value, while WC–Co hardmetal shows the higher value. The variation of i_{corr} value could be explained from the following reasons. The main reason was the formation of dense passivation film on the surface of WC–Al$_2$O$_3$ composite, which could decrease the corrosion rate of the composites. In addition, the i_{pass} of WC–Al$_2$O$_3$ composite is lower than WC–Co hardmetal. In short, it can be concluded that WC–Al$_2$O$_3$ composites had more positive E_{corr} value, lower i_{corr} and i_{pass} values, indicating that WC–Al$_2$O$_3$ composites possessed better corrosion resistance in NaCl solution from corrosion thermodynamics and corrosion kinetics.

3.3.3 EIS analysis. Fig. 7 presents the EIS results of WC-based composites in NaCl solution. The Nyquist spectrum of all the composites in NaCl solution both have similar capacitive loops (Fig. 7(a) and (d)), which indicate that both of two composites have similar corrosion processes. The capacitive arc radius of the Nyquist plots at low frequencies can reflect the corrosion resistance of the materials. Hence, it could be inferred that WC–Al$_2$O$_3$ composites possesses higher corrosion resistance than WC–Co hardmetal owing to the larger capacitive loop of WC–Al$_2$O$_3$ composite. The results are consistent with the polarization results. As presented in Fig. 7(b) and (e),

the impedance value of WC–Al$_2$O$_3$ composite increases more rapidly than WC–Co hardmetal during the 24 hours, which indicates that WC–Al$_2$O$_3$ composite possesses more compacted passivation film than WC–Co hardmetal. The passivation film on the surface of WC–Al$_2$O$_3$ composite could inhibit further corrosion of the inner material. However, the impedance value of WC–Co cemented carbide showed no obvious change with the increasing of testing time. It implies that the passive film of WC–6Co cemented carbide cannot protect inner material to avoid further corrosion. According to the Bode results (Fig. 7(c) and (f)), the impedance of WC matrix composite was fitted by two time constants, one of which was related to the corrosion process at low frequencies, and the other was related to the passivation layer at high frequencies.[36] The phase angle curves of WC–Al$_2$O$_3$ composite are closer to the low-frequency region than WC–Co cemented carbide. Kellner et al.[21] also been reported that a wider phase angle curve means an improved corrosion resistance of the materials.

Fig. 7(g) presents the equivalent circuit of WC-based composites. In the circuit, R_{ct} is the resistance of charge transfer; R_s and R_f represent the resistances of corrosion solution and corrosion products, respectively; Q_f and Q_{ct} are the capacitances of corrosion products and double-charge layer, respectively. The corrosion parameters of WC-based composites during corrosion process were presented in Table 3. The variations in Q_f and R_f occur on the composites and reflect the growth of passivation film on the surface of the composites. Compared with WC–Co cemented carbide, the values of decreased Y_0 (Q_f) of WC–Al$_2$O$_3$ composite in NaCl solution showed more compacted passivation film on the surface of the composites.[32] The value of Q_{ct} in NaCl solution was higher than the typical of a double layer (1–100 µF cm^{-2}). This phenomenon could be explained by an increase in the number of corrosion products (oxides), which will expand the electrochemical active region, if semiconducting, the double layer could be formed. The most significant corrosion parameter for the composite is the charge transfer resistance (R_{ct}), which is related to Faraday process and it can reflect the corrosion rate of the materials. The higher the R_{ct}, the higher resistance to corrosion. The R_{ct} value of WC–Co cemented carbide in NaCl solution was lower than WC–Al$_2$O$_3$ composites. In addition, the polarization resistance (R_p) is shown in Fig. 7(h). The polarization resistance (R_p) is equal to the sum of the corrosion product films resistance (R_f) and charge transfer resistance (R_{ct}).[29,41] The R_p value of WC–Al$_2$O$_3$ composite is about one order of magnitude higher than WC–Co cemented carbide. As the increase of corrosion time, the R_p value of WC–Al$_2$O$_3$ composites increased obviously. However, for WC–Co cemented carbide, R_p value keeps a stable value. Therefore, it could be concluded that compared with WC–Co cemented carbide, WC–Al$_2$O$_3$ composites has higher corrosion resistance. The EIS result is consistent with the polarization curve and the weight-loss result.

3.4 Characterization of the corroded surface

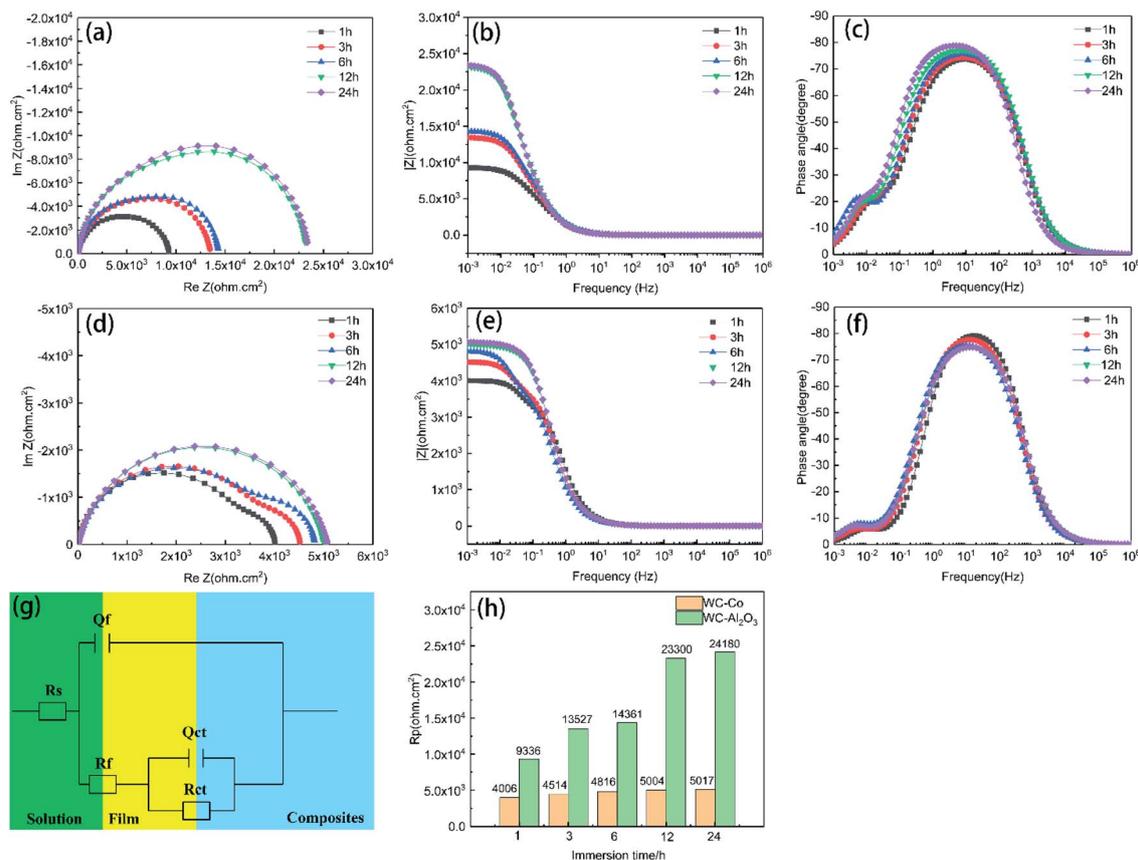**3.4.1 Corrosion morphologies.** Fig. 8 presents the typical SEM images of WC–Co cemented carbide and WC–Al$_2$O$_3$

Fig. 7 The EIS results of WC–Al$_2$O$_3$ (a–c) and WC–Co (d–f), equivalent circuit (g) and R_p (h).

composite before and after potentiodynamic polarization tests, respectively. Fig. 9 and 10 show the EDS analysis results of corrosion products for WC–Co cemented carbide and WC–Al$_2$O$_3$ composite after potentiodynamic polarization tests, respectively. As shown in Fig. 8, the remarkable distinctions can be found between the polished specimens and the corroded specimens. As presented in Fig. 8(b), a large number of loose corrosion products and many pores can be seen on the surface of WC–Co cemented carbide, which means that the electrolyte solution could penetrate the loose corrosion products and

accelerate further corrosion of the material. During the SEM and EDS analysis, the surface was sprayed with Pt element. The original data includes Pt elements and cannot be deleted, but it does not affect the analysis of the results. According to the EDS analysis results of WC–Co cemented carbide, as shown in Fig. 10, W, C, Co, O exist on the corroded surface, which is attributed to the formation of oxide compounds. It also can be inferred that cobalt is far more corrosive than tungsten in NaCl solution. Ali Fazili et al.[37] has reported that Co binder was preferentially dissolved, subsequently a part of WC particles was

Table 3 EIS fitting parameters of WC–Al$_2$O$_3$ and WC–Co samples

| Samples | Time/h | R_s (Ω cm^2) | Q_f | | R_f (Ω cm^2) | Q_{ct} | | R_{ct} (Ω cm^2) | R_p (Ω cm^2) |
			Y_0 (μF cm^{-2})	n		Y_0 (μF cm^{-2})	n		
WC–15Al$_2$O$_3$	1	7.38	133.4	0.86	7116	1299	0.91	2220	9336
	3	7.09	133.1	0.86	10 270	1239	0.99	3257	13 527
	6	6.95	129.8	0.87	10 460	1174	1	3901	14 361
	12	6.77	127.9	0.90	16 250	799	1	7050	23 300
	24	6.81	118.6	0.90	16 851	608	1	7329	24 180
WC–6Co	1	5.29	97.2	0.93	3389	6447	1	617	4006
	3	5.37	127.9	0.91	3817	9211	1	697	4514
	6	5.45	140.4	0.88	3878	8177	1	937	4815
	12	5.30	141.6	0.88	4059	66.99	1	945	5004
	24	5.30	168	0.88	4139	65.82	1	932	5071

© 2021 The Author(s). Published by the Royal Society of Chemistry
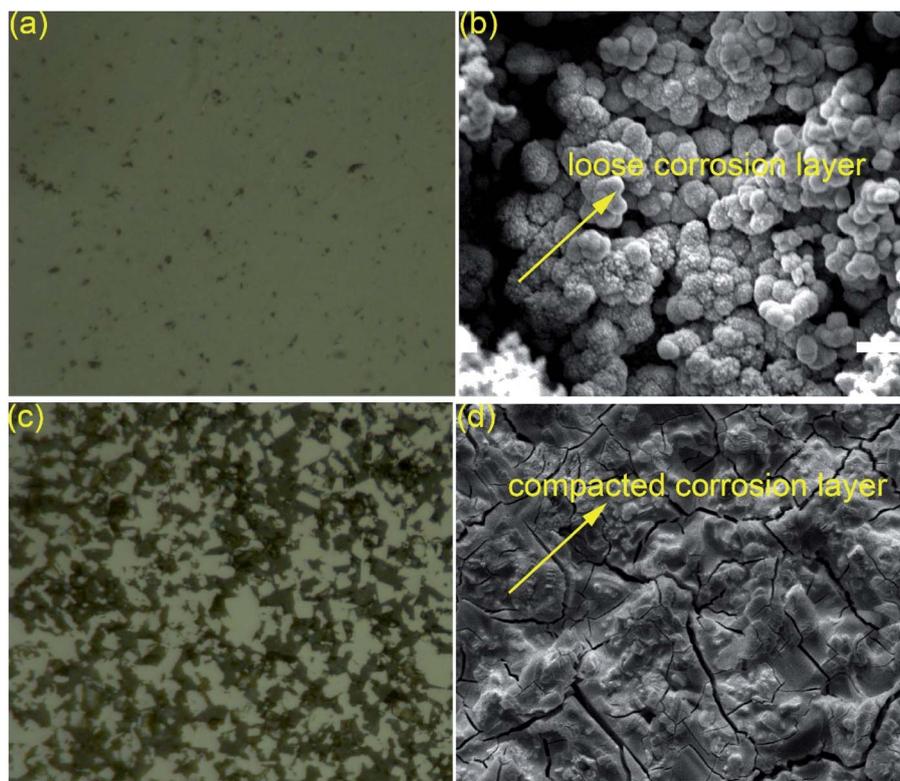
Fig. 8 Typical SEM morphologies of the specimens before and after potentiodynamic polarization tests: (a) initial polished sample for WC−Co; (b) corroded sample for WC−Co; (c) initial polished sample for WC−Al$_2$O$_3$; (d) corroded sample for WC−Al$_2$O$_3$.
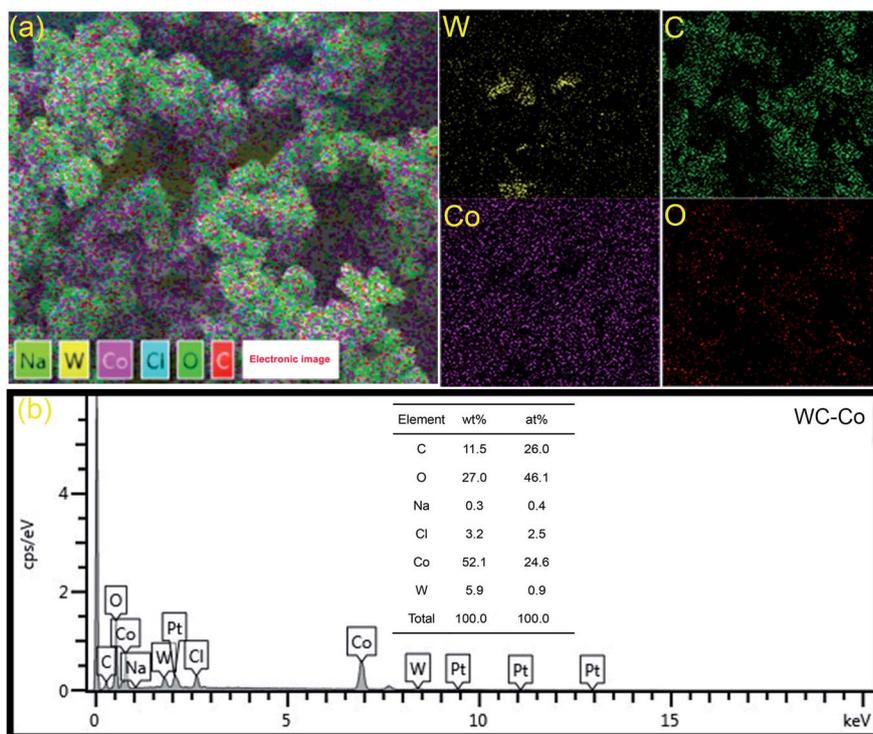

Fig. 9 (a) EDS mapping scanning of WC−Co cemented carbide; (b) element quantitative analysis of WC−Co hard metal after potentiodynamic polarization tests.
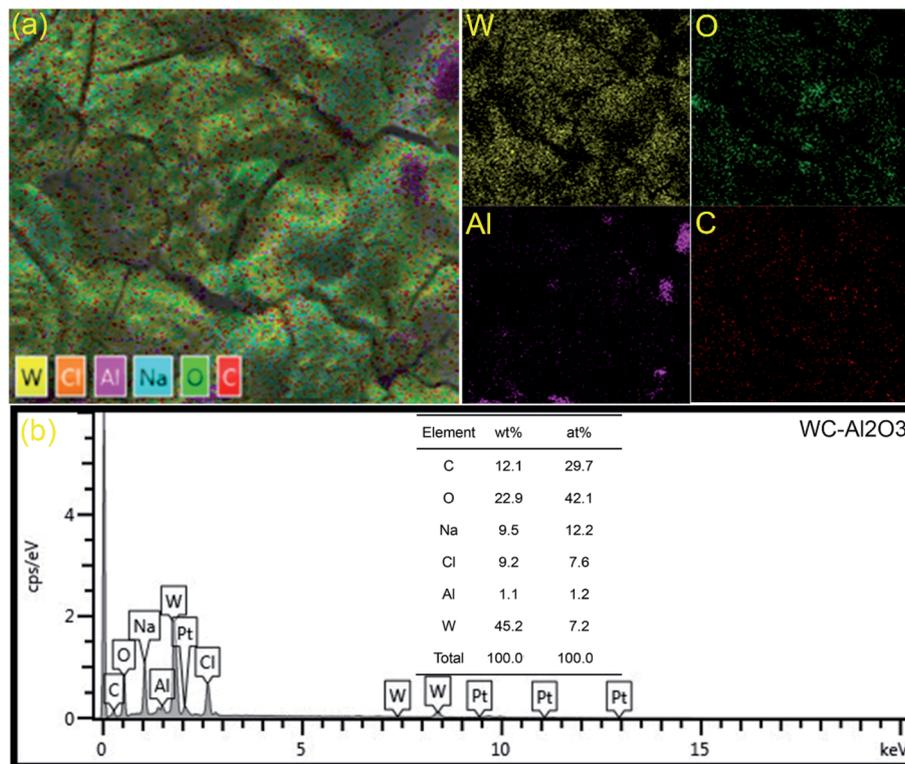
Fig. 10 (a) EDS mapping scanning of WC–Al$_2$O$_3$ composite; (b) element quantitative analysis of WC–Al$_2$O$_3$ composite after potentiodynamic polarization tests.
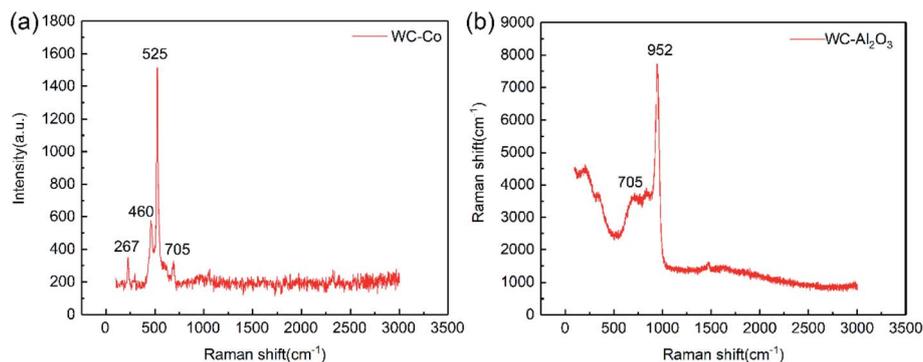

Fig. 11 The Raman results of the composites after potentiodynamic polarization tests: (a) WC–Co; (b) WC–Al$_2$O$_3$.

corroded in NaCl solution. Since EDS analysis is a semi-qualitative characterization method and cannot accurately determine the composition of corrosion products, other characterization methods are needed. Combined with Raman, EDS and XPS results, the composition of corrosion products can be strictly determined.

Turning to WC–Al$_2$O$_3$ composite, as presented in Fig. 8(b) and (d), different corrosion morphologies were observed on the surface of WC–Co cemented carbide and WC–Al$_2$O$_3$ composites. As presented in Fig. 8(d), the compacted passive film was formed on the surface of WC–Al$_2$O$_3$ composite. According to the EDS results of WC–Al$_2$O$_3$ composite (Fig. 11), it could be found that the main elements are W and O, which could correspond in EDS mapping. The O content of the original composite is only

15 wt%, but the O content increases after potentiodynamic polarization tests. Hence, it could be speculated that the corrosion products of WC–Al$_2$O$_3$ composites contains WO$_3$.

3.4.2 Raman and XPS results. Fig. 11 presents the Raman spectra of WC–Co cemented carbide and WC–Al$_2$O$_3$ composites after potentiodynamic polarization tests. As illustrated in Fig. 11(a), the positions of the main peak on the surface of WC–Co hard metal are 267 cm^{-1} (WO$_3$), 705 cm^{-1} (WO$_3$), 460 cm^{-1} (Co(OH)$_2$), 525 cm^{-1} (Co$_3$O$_4$),[15,39,40] indicating that the corrosion process of WC–Co cemented carbide is attributed to the preferential dissolution of Co binder and the oxidation of WC phase. However, as presented in Fig. 11(b), the positions of the main peak on the surface of WC–Al$_2$O$_3$ composites are 952 cm^{-1} (WO$_3$) and 705 cm^{-1} (WO$_3$),[32,38–40] indicating that the corrosion

product of WC–Al$_2$O$_3$ composites contains mainly tungsten oxide. In addition, the Raman results in this work are consistent with the previous literature by Konadu et al. and Zhang et al.[20,38]

Fig. 12 and 13 show the XPS results of WC–Co cemented carbide and WC–Al$_2$O$_3$ composites after potentiodynamic polarization tests, respectively. As illustrated in Fig. 12(a), the peaks of W, Co, O and C could be identified in the XPS spectra of WC–Co cemented carbide. The peaks of Co 2p were determined as Co(OH)$_2$ and Co$_3$O$_4$ (Fig. 12(b)), which is in agreement with the results by Li Zhang et al.[18,20] The W 4f peaks corresponded to WC and WO$_3$ (Fig. 12(c)), which implies that WC phase was also suffered certain corrosion after Co binder was dissolved. The C 1s peaks were associated with WC (Fig. 12(d)). The peaks of O 1s corresponded to WO$_3$, Co(OH)$_2$ and Co$_3$O$_4$ (Fig. 12(c)). As illustrated in Fig. 13(a), the peaks of W, Al, O and C elements can be detected in the XPS spectra of WC–Al$_2$O$_3$ composite. The peak of Al 2p correspond to Al$_2$O$_3$ (Fig. 13(b)). Based on W 4f and O 1s, the result indicated that the peak was determined as WO$_3$ (Fig. 13(c) and (d)). It could be inferred that the oxidation reaction of WC phased occurred at the anode. Zhang et al.[20] reported that the corrosion product of WC–Co in acidic solution is also WO$_3$. The peak of C 1s was determined as WC (Fig. 13(e)). Hence, it could be concluded that the corrosion product of WC–Al$_2$O$_3$ composites is WO$_3$, which is in agreement with EDS and Raman results.

3.5 Corrosion mechanism

Fig. 14 displays the corrosion current transients of WC–Co cemented carbide and WC–Al$_2$O$_3$ composites in NaCl solution. The applied potentials were −300 and 750 mV vs. SCE in the passivation region for WC–Co and WC–Al$_2$O$_3$ composite, respectively. With the increase of corrosion time, the corrosion current

density decreased to a stable value, and the potentiostatic polarization behavior of WC–Al$_2$O$_3$ and WC–Co composite was analyzed. Lekatou et al.[41] believed that the current density increased and stabilized to a stable value with immersion time, indicating that the passivation behavior of the material has occurred. As shown in Fig. 14(a) and (b), WC–Co cemented carbide shows the greatest steady current density value with the increasing immersion time, implying that the corrosion behavior of WC–Co cemented carbide is general corrosion corresponding with the dissolution of Co binder. However, as shown in Fig. 14(c) and (d), the current density of WC–Al$_2$O$_3$ composites indicated an obvious fluctuation, which implied that the passivation film of WC–Al$_2$O$_3$ composites was broken in NaCl solution. Hence, it could be inferred that the corrosion behavior of WC–Co cemented carbide in NaCl solution is general corrosion by the dissolution of Co binder, but for WC–Al$_2$O$_3$ composites is general corrosion by the oxidation of WC phase and the dissolution of Al$_2$O$_3$ phase.

Fig. 15 shows the schematic illustrations of the corrosion mechanism for WC–Co cemented carbide and WC–Al$_2$O$_3$ composite, respectively. As presented in Fig. 15(a1), after removing the loose corrosion products, WC skeleton is left, which imply that Co binder has been dissolved. Combined with EDS, XPS and Raman analysis, it can be further confirmed that the corrosion behavior of WC–Co cemented carbide in NaCl solution exhibits general corrosion characteristic. Katiyar et al.[31] have reported that Co binder plays cathodic protection role for WC phase, which inhibit the corrosion of WC phase. However, when Co binder was totally dissolved, subsequently WC phase was also oxidized to WO$_3$. Therefore, the corrosion mechanism of WC–Co cemented carbide in NaCl solution is the electrochemical dissolution of Co binder and the chemical oxidation of WC phase.
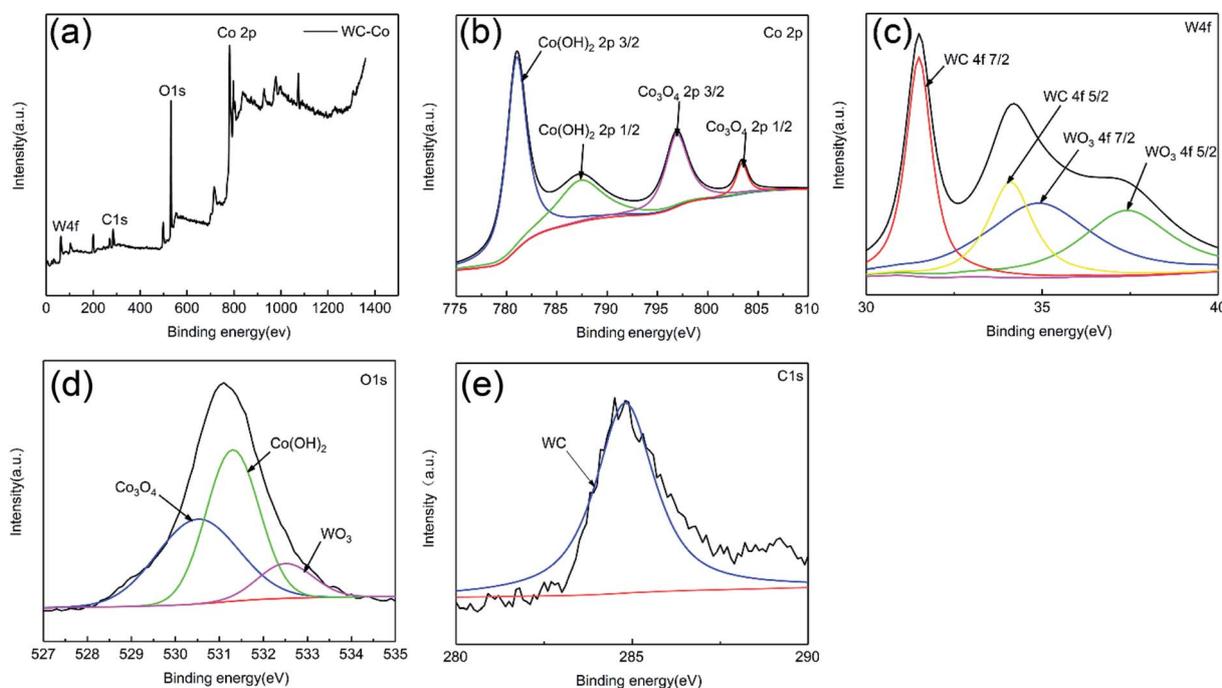

Fig. 12   XPS spectra of corroded surface of WC–Co cemented carbide after potentiodynamic polarization tests: (a) wide scan survey spectra, (b) Co 2p, (c) W 4f, (d) O 1s, (e) C 1s.
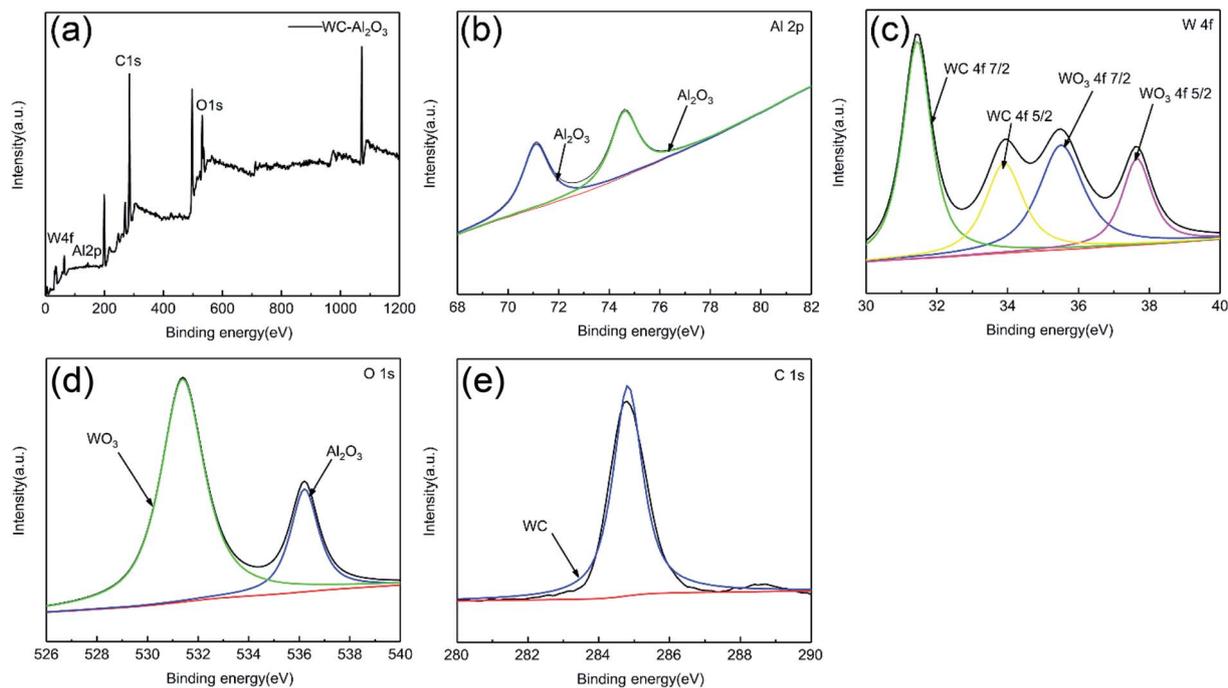
Fig. 13 XPS results of WC−Al$_2$O$_3$ composite after potentiodynamic polarization tests: (a) survey spectrum, (b) Al 2p, (c) W 4f, (d) O 1s, (e) C 1s.

As written in Reaction (1), Co binder would react with water to form CoO.[17]

$$Co + H_2O \rightarrow CoO + 2H^+ + 2e^- \quad (1)$$

This is oxidized to Co$_3$O$_4$, which is the final product. Therefore, CoO is not detected by Raman and XPS. This process can be expressed as the following reactions:
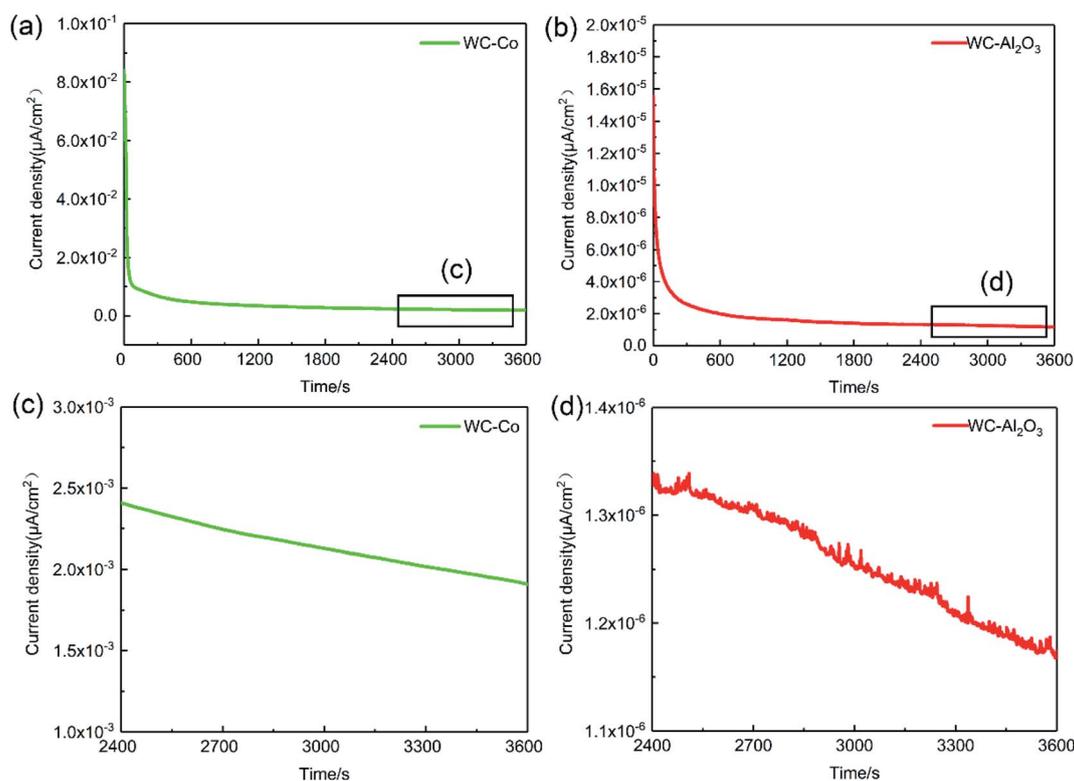
$$3CoO + H_2O \rightarrow Co_3O_4 \text{ (corrosion products)} + 2H^+ + 2e^- \quad (2)$$

Fig. 14 Current transients of WC−Co (a and c) and WC−Al$_2$O$_3$ (b and d) composites at passivation region in NaCl solution.
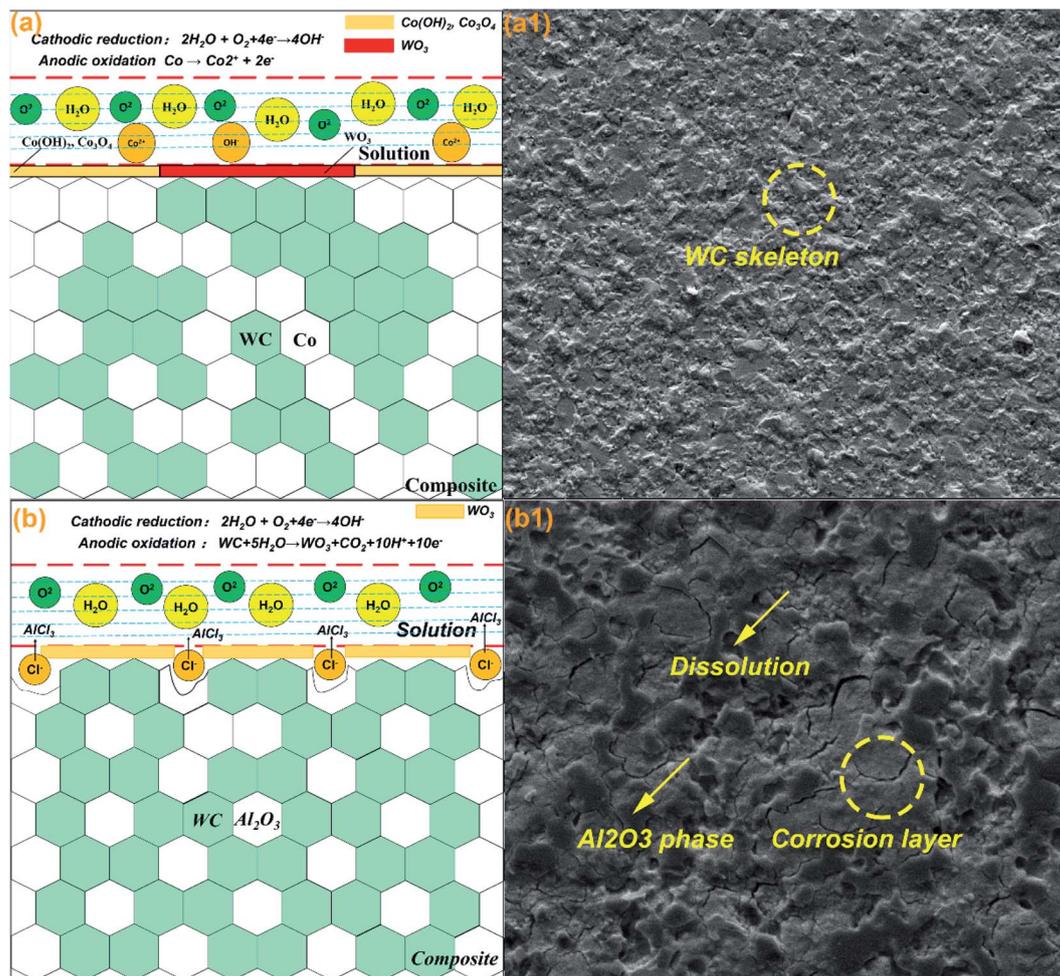
Fig. 15 Schematic diagram of corrosion mechanism after potentiodynamic polarization tests: (a and a1) WC–Co; (b and b1) WC–Al$_2$O$_3$.

In addition, the most significant corrosion process for WC–Co cemented carbide is, respectively, cobalt dissolution of the anode and oxygenation reaction of the cathode. The reactions are as follows:[33]

$$Co \rightarrow Co^{2+} + 2e^- \tag{3}$$

$$2H_2O + O_2 + 4e^- \rightarrow 4OH^- \tag{4}$$

Then, the OH$^-$ ions react with Co^{2+} ions to form cobalt hydroxide:

$$Co^{2+} + 2OH^- \rightarrow Co(OH)_2 \text{ (corrosion products)} \tag{5}$$
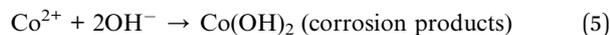
After Co binder is dissolved, WC phase exposed to NaCl solution begins to corrode. The reaction is as follows:[29]

$$WC + 5H_2O \rightarrow WO_3 \text{ (corrosion products)} + CO_2 + 10H^+ + 10e^- \tag{6}$$
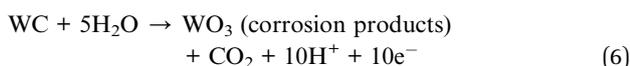
As presented in Fig. 15(b1), after removing the loose corrosion products, the compacted corrosion layer is still on the surface of WC–Al$_2$O$_3$ composites. In addition, the corroded surface of WC–Al$_2$O$_3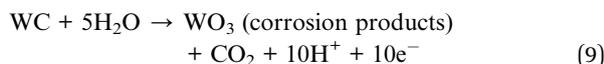$ composite showed some cracks, which may be caused by stress due to the polarization process and new phase formation.[42] Combined with EDS, XPS and Raman analysis, it can be inferred that the corrosion behavior of WC–Al$_2$O$_3$ composites exhibit the general corrosion characteristic. The corrosion of WC phase can cause the spalling of Al$_2$O$_3$ phase. Sudha *et al.* and Ouyang *et al.*[28,43] confirmed that ceramic phase (such as Al$_2$O$_3$ and MgO) is a good insulator, and WC phase has excellent conductivity, so WC phase cannot form a galvanic couple with Al$_2$O$_3$ phase. Loto *et al.*[44] reported that chemical corrosion occurred on the surface of Al$_2$O$_3$ phase. Hence, the corrosion process of WC–Al$_2$O$_3$ composites is the electrochemical oxidation of WC phase and the chemical dissolution of Al$_2$O$_3$ phase in NaCl solution. As expressed in Reaction (7), leading to the high hydration of surface film.[44]

$$Al_2O_3 + 3H_2O \rightarrow 2Al(OH)_3 \tag{7}$$
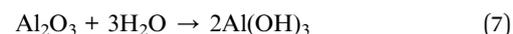
The adsorption of Cl$^-$ onto the WC–Al$_2$O$_3$ composite easily transforms Al(OH)$_3$ to soluble AlCl$_3$. Diffusion of AlCl$_3$ from the surface of samples to electrolyte leads to the corrosion of WC–Al$_2$O$_3$ composite.[44]

$$Al(OH)_3 + 2Cl^- \rightarrow AlCl_3 + 2OH^- \tag{8}$$
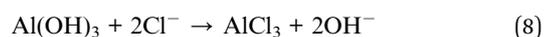
The most important anodic and cathodic processes of WC–Al_2O_3 composites are tungsten carbide oxidation of the anode and oxygenation reaction of the cathode in NaCl solution, respectively. The specific electrochemical reaction is as follows:

$$WC + 5H_2O \rightarrow WO_3 \text{ (corrosion products)}$$
$$+ CO_2 + 10H^+ + 10e^- \qquad (9)$$

$$2H_2O + O_2 + 4e^- \rightarrow 4OH^- \qquad (10)$$

In summary, combined with the results of polarization curve, it could be rigorously inferred that the corrosion current density increased during anodic polarization due to the oxidation of WC phase. WC–Al_2O_3 composite could form the compacted passivation film after corrosion test in NaCl solution. Hence, it could be confirmed that the corrosion resistance of WC–Al_2O_3 composite is higher than WC–Co cemented carbide.

4. Conclusion

In this work, the corrosion behavior of WC–Al_2O_3 composite and WC–Co cemented carbide in NaCl solution were investigated by immersion corrosion test and electrochemical test. Some important conclusions are as follows:

(1) WC–Al_2O_3 composites has higher corrosion resistance than WC–Co cemented carbide in NaCl solution, due to the lower i_{corr} and more positive E_{corr} for WC–Al_2O_3 composites. In addition, the corrosion current density is different from the passivation current density, indicating the passivation trend. The pseudo-passivation of WC–Co cemented carbide was observed in NaCl solution ($i_{pass} \gg 10\ \mu A\ cm^{-2}$). However, WC–$Al_2O_3$ composite exhibited the passivation behavior ($i_{pass} < 10\ \mu A\ cm^{-2}$).

(2) The EIS results also proved higher corrosion resistance of WC–Al_2O_3 composite, due to the higher value of polarization resistance (R_p). The impedance value of WC–Al_2O_3 composite increased more rapidly than WC–Co cemented carbide, indicating that compacted passivation film was formed on the surface of WC–Al_2O_3 composites, and its stability and compactness was enhanced with the increase of immersion time.

(3) The corrosion behavior of conventional WC–Co cemented carbide is general corrosion with preferential dissolution of Co binder and subsequent oxidation of WC phase. The corrosion products of WC–Co cemented carbide contain mainly $Co(OH)_2$, Co_3O_4 and a small amount of WO_3. In addition, the corrosion mechanism of WC–Al_2O_3 composite is general corrosion, in which WC phase is oxidized and a small amount of Al_2O_3 phase is dissolved. The corrosion products of WC–Al_2O_3 composites contain mainly WO_3.

Conflicts of interest

There are no conflicts to declare.

Acknowledgements

References

1 P. K. Katiyar, P. K. Singh, R. Singh and A. L. Kumar, Modes of failure of cemented tungsten carbide tool bits (WC/Co): A study of wear parts, *Int. J. Refract. Met. Hard Mater.*, 2016, **54**, 27–38.

2 C. L. Cramer, T. G. Aguirre, N. R. Wieber, R. A. Lowden, A. A. Trofimov, H. Wang, J. Yan, M. P. Paranthaman and A. M. Elliott, Binder jet printed WC infiltrated with pre-made melt of WC and Co, *Int. J. Refract. Met. Hard Mater.*, 2020, **87**, 105137.

3 X. Liu, X. Song, H. Wang, X. Liu, F. Tang and H. Lu, Complexions in WC–Co cemented carbides, *Acta Mater.*, 2018, **149**, 164–178.

4 Q. Yang, J. Yang, H. Yang and J. Ruan, The effects of fine WC contents and temperature on the microstructure and mechanical properties of inhomogeneous WC-(fine WC–Co) cemented carbides, *Ceram. Int.*, 2016, **42**(16), 18100–18107.

5 X. Zhang, S. Zhu, T. Shi, H. Ding, Y. Bai and P. Di, Preparation, mechanical and tribological properties of WC–Al_2O_3 composite doped with graphene platelets, *Ceram. Int.*, 2020, **46**(8, Part A), 10457–10468.

6 R. Useldinger and U. Schleinkofer, Creep behaviour of cemented carbides—Influence of binder content, binder composition and WC grain size, *Int. J. Refract. Met. Hard Mater.*, 2017, **62**, 170–175.

7 J. Li, J. Cheng, P. Chen, W. Chen and C. Wei, Fabrication of WC–Co cemented carbides with gradient distribution of WC grain size and Co composition by lamination pressing and microwave sintering, *Ceram. Int.*, 2018, **44**(10), 11225–11232.

8 Q. Yang, S. Yu, C. Zheng, J. Liao, J. Li, L. Chen, *et al.* Effect of carbon content on microstructure and mechanical properties of WC–10Co cemented carbides with plate-like WC grain, *Ceram. Int.*, 2020, **46**(2), 1824–1829.

9 Q. Zhang, N. Lin and Y. He, Effects of Mo additions on the corrosion behavior of WC–TiC–Ni hardmetals in acidic solutions, *Int. J. Refract. Met. Hard Mater.*, 2013, **38**, 15–25.

10 H. Qu, S. Zhu, Q. Li and C. Ouyang, Microstructure and mechanical properties of hot-pressing sintered WC–x vol.% Al_2O_3 composites, *Mater. Sci. Eng., A*, 2012, **543**, 96–103.

11 H. Qu, S. Zhu, Q. Li and C. Ouyang, Influence of sintering temperature and holding time on the densification, phase transformation, microstructure and properties of hot-pressing WC–40 vol.%Al_2O_3 composites, *Ceram. Int.*, 2012, **38**(2), 1371–1380.

12 W. Dong, S. Zhu, T. Bai and Y. Luo, Influence of Al_2O_3 whisker concentration on mechanical properties of WC–Al_2O_3 whisker composite, *Ceram. Int.*, 2015, **41**(10), 13685–13691.

13 H. Qu and S. Zhu, Two step hot pressing sintering of dense fine-grained WC–Al_2O_3 composites, *Ceram. Int.*, 2013, **39**(5), 5415–5425.

14 H. Qu, S. Zhu, P. Di, C. Ouyang and Q. Li, Microstructure and mechanical properties of WC–40vol%Al_2O_3 composites hot

pressed with MgO and CeO_2 additives, *Ceram. Int.*, 2013, **39**(2), 1931–1942.

15 W. Dong, S. Zhu, H. Qu and X. Liu, Microstructural evolution and mechanical properties of hot-pressed WC–α-Al_2O_3 with Y_2O_3 and CeO_2, *Adv. Appl. Ceram.*, 2016, **115**(6), 316–321.

16 W. Dong, S. Zhu, Y. Wang and T. Bai, Influence of VC and Cr_3C_2 as grain growth inhibitors on WC–Al_2O_3 composites prepared by hot press sintering, *Int. J. Refract. Met. Hard Mater.*, 2014, **45**, 223–229.

17 Q. Su, S. Zhu, H. Ding, Y. Bai and P. Di, Effect of the additive VC on tribological properties of WC–Al_2O_3 composites, *Int. J. Refract. Met. Hard Mater.*, 2018, **75**, 111–117.

18 H. Scholl, B. Hofman and A. Rauscher, Anodic polarization of cemented carbides of the type [(WC, M): M = Fe, Ni or Co] in sulphuric acid solution, *Electrochim. Acta*, 1992, **37**(3), 447–452.

19 A. Ismail and N. Abd Aziz, Corrosion behavior of WC–Co and WC–Ni in 3.5% NaCl at increasing temperature, *Appl. Mech. Mater.*, 2014, **660**, 135–139.

20 L. Zhang, Y. Chen, Q. Wan, T. Liu, J. Zhu and W. Tian, Electrochemical corrosion behaviors of straight WC–Co alloys: Exclusive variation in grain sizes and aggressive media, *Int. J. Refract. Met. Hard Mater.*, 2016, **57**, 70–77.

21 F. J. J. Kellner, H. Hildebrand and S. Virtanen, Effect of WC grain size on the corrosion behavior of WC–Co based hardmetals in alkaline solutions, *Int. J. Refract. Met. Hard Mater.*, 2009, **27**(4), 806–812.

22 W. J. Tomlinson and N. J. Ayerst, Anodic polarization and corrosion of WC–Co hardmetals containing small amounts of Cr_3C_2 and/or VC, *J. Mater. Sci.*, 1989, **24**, 2348–2352.

23 A. M. Human and H. E. Exner, Electrochemical behaviour of tungsten-carbide hardmetals, *Mater. Sci. Eng., A*, 1996, **209**(1), 180–191.

24 L. Zhang, Y. Feng, Q. Nan, R. Ke, Q. Wan and Z. Wang, Effects of titanium-based raw materials on electrochemical behavior of Ti(C,N)-based cermets, *Int. J. Refract. Met. Hard Mater.*, 2015, **48**, 11–18.

25 F. J. J. Kellner, M. S. Killian, G. Yang, E. Spiecker and S. Virtanen, TEM and ToF-SIMS studies on the corrosion behavior of vanadium and chromium containing WC–Co hard metals in alkaline solutions, *Int. J. Refract. Met. Hard Mater.*, 2011, **29**(3), 376–383.

26 A. M. Human and H. E. Exner, The relationship between electrochemical behaviour and in-service corrosion of WC based cemented carbides, *Int. J. Refract. Met. Hard Mater.*, 1997, **15**(1), 65–71.

27 Y. Ma, L. Zhang, C. Shan, T. Lei and X. Cheng, Electrochemical corrosion behaviors of binderless carbides, *Fenmo Yejin Cailiao Kexue yu Gongcheng/Materials Science and Engineering of Powder Metallurgy*, 2011, **16**(6), 820–826.

28 C. Ouyang, S. Zhu and D. Y. Li, Corrosion and corrosive wear behavior of WC–MgO composites with and without grain-growth inhibitors, *J. Alloys Compd.*, 2014, **615**, 146–155.

29 S. Hochstrasser Kurz, Y. Mueller, C. Latkoczy, S. Virtanen and P. Schmutz, Analytical characterization of the corrosion mechanisms of WC–Co by electrochemical

30 S. Sutthiruangwong and G. Mori, Corrosion properties of Co-based cemented carbides in acidic solutions, *Int. J. Refract. Met. Hard Mater.*, 2003, **21**(3), 135–145.

31 P. K. Katiyar and N. S. Randhawa, Corrosion behavior of WC–Co tool bits in simulated (concrete, soil, and mine) solutions with and without chloride additions, *Int. J. Refract. Met. Hard Mater.*, 2019, **85**, 105062.

32 L. Wei, Y. Liu, Q. Li and Y. F. Cheng, Effect of roughness on general corrosion and pitting of $(FeCoCrNi)_{0.89}(WC)_{0.11}$ high-entropy alloy composite in 3.5 wt.% NaCl solution, *Corros. Sci.*, 2019, **146**, 44–57.

33 A. Fazili, M. R. Derakhshandeh, S. Nejadshamsi, L. Nikzad, M. Razavi and E. Ghasali, Improved electrochemical and mechanical performance of WC–Co cemented carbide by replacing a part of Co with Al_2O_3, *J. Alloys Compd.*, 2020, **823**, 153857.

34 J. B. Sun, G. A. Zhang, W. Liu and M. X. Lu, The formation mechanism of corrosion scale and electrochemical characteristic of low alloy steel in carbon dioxide-saturated solution, *Corros. Sci.*, 2012, **57**, 131–138.

35 M. H. Martin and A. Lasia, Influence of experimental factors on the constant phase element behavior of Pt electrodes, *Electrochim. Acta*, 2011, **56**(23), 8058–8068.

36 A. M. F. Rocha, A. C. Bastos, J. P. Cardoso, F. Rodrigues, C. M. Fernandes, E. Soares, J. Sacramento, A. M. R. Senos and M. G. S. Ferreira, Corrosion behaviour of WC hardmetals with nickel-based binders, *Corros. Sci.*, 2019, **147**, 384–393.

37 A. Fazili, M. R. Derakhshandeh, S. Nejadshamsi, L. Nikzad, M. Razavi and E. Ghasali, Improved electrochemical and mechanical performance of WC–Co cemented carbide by replacing a part of Co with Al_2O_3, *J. Alloys Compd.*, 2020, **823**, 153857.

38 D. S. Konadu, J. V. D. Merwe, J. H. Potgieter, S. Potgieter-Vermaak and C. N. Machio, The corrosion behaviour of WC–VC–Co hardmetals in acidic media, *Corros. Sci.*, 2010, **52**(9), 3118–3125.

39 M. Arai, S. Hayashi, K. Yamamoto and S. S. Kim, Raman studies of phase transitions in gas-evaporated WO_3 microcrystals, *Solid State Commun.*, 1990, **75**(7), 613–616.

40 K. Ç. Demir, Corrosion behavior of electrodeposited WO_3 thin films, *Ceram. Int.*, 2020, **46**(4), 4358–4364.

41 A. Lekatou, E. Regoutas and A. E. Karantzalis, Corrosion behaviour of cermet-based coatings with a bond coat in 0.5 M H_2SO_4, *Corros. Sci.*, 2008, **50**(12), 3389–3400.

42 S. Guo, R. Bao, J. Yang, H. Chen and J. Yi, Effect of Mo and Y_2O_3 additions on the microstructure and properties of fine WC–Co cemented carbides fabricated by spark plasma sintering, *Int. J. Refract. Met. Hard Mater.*, 2017, **69**, 1–10.

43 P. N. Sudha, *Fundamental Biomaterials: Ceramics‖Corrosion of Ceramic Materials*, 2018.

44 R. T. Loto and A. Adeleke, Corrosion of Aluminum Alloy Metal Matrix Composites in Neutral Chloride Solutions, *Journal of Failure Analysis and Prevention*, 2016, **16**(5), 874–885.

methods and inductively coupled plasma mass spectroscopy, *Corros. Sci.*, 2007, **49**(4), 2002–2020.